Hindawi Publishing Corporation
International Journal of Distributed Sensor Networks
Volume 2012, Article ID 191235, 12 pages
doi:10.1155/2012/191235

Research Article

Constructing a Distributed AUV Network for Underwater Plume-Tracking Operations

Stephanie Petillo, Henrik Schmidt, and Arjuna Balasuriya

Laboratory for Autonomous Marine Sensing Systems, Department of Mechanical & Ocean Engineering, Massachusetts Institute of Technology, Room 5-204, 77 Massachusetts Avenue, Cambridge, MA 02139, USA

Correspondence should be addressed to Stephanie Petillo, spetillo@mit.edu

Received 1 June 2011; Revised 26 August 2011; Accepted 6 September 2011

Academic Editor: Don Sofge

In recent years, there has been significant concern about the impacts of offshore oil spill plumes and harmful algal blooms on the coastal ocean environment and biology, as well as on the human populations adjacent to these coastal regions. Thus, it has become increasingly important to determine the 3D extent of these ocean features ("plumes") and how they evolve over time. The ocean environment is largely inaccessible to sensing directly by humans, motivating the need for robots to intelligently sense the ocean for us. In this paper, we propose the use of an autonomous underwater vehicle (AUV) network to track and predict plume shape and motion, discussing solutions to the challenges of spatiotemporal data aliasing (coverage versus resolution), underwater communication, AUV autonomy, data fusion, and coordination of multiple AUVs. A plume simulation is also developed here as the first step toward implementing behaviors for autonomous, adaptive plume tracking with AUVs, modeling a plume as a sum of Fourier orders and examining the resulting errors. This is then extended to include plume forecasting based on time variations, and future improvements and implementation are discussed.

1. Introduction

The underwater environment itself is hazardous to humans, as we cannot survive without air to breathe and our bodies cannot withstand the ambient pressure deep underwater, yet we could not exist without the presence of large bodies of water on our planet. The health of the oceans has a significant impact on both marine and human life. This has been observed most recently through the impact of offshore oil spill plumes and harmful algal blooms (HABs) on coastal waters. However, even in healthy ocean conditions, the ocean environment can be dangerous for humans, such as near the extreme temperatures and chemicals spewing out of hydrothermal vents into fluid clouds deep in the ocean. These features of the ocean environment create a challenge for underwater exploration and oceanographic data collection. The use of autonomous (unmanned) underwater vehicles (AUVs) in such environments is crucial to safely and efficiently completing these tasks, as they can be designed to withstand biological and chemical contaminants, high pressures, and extreme temperature variations. AUVs (especially actively propelled ones) can also be programmed to react autonomously and adaptively to changes in their environments by controlling their own motion, unlike drifters, moored sensing arrays, or sensing buoys.

Oil spill plumes, HABs, and clouds of hydrothermal vent fluid in particular can each be viewed as a type of underwater plume (much like a cloud or plume of smoke), evolving in 3D space and over time. These plumes can range in scale from tens of meters to hundreds of kilometers in horizontal space at their neutrally buoyant depths and move with the prevailing currents as well as spread and diffuse into the surrounding water masses [1, 2]. Trying to track meso- and large-scale features (as plumes often are) with relatively small AUVs requires the coordinated effort of multiple AUVs, due largely to both battery life and AUV speed limitations. Willcox et al. [3] take a unique approach to this challenge in which they determine an optimal AUV survey and sampling strategy by quantifying an AUV's energy efficiency, quantifying the degree of synopticity with which an AUV can measure an ocean process, and accounting for inherent survey errors in the sampling strategy. Plume tracking also

brings forth the problem of spatiotemporal aliasing of data when the plume is too large and/or moving too fast for a single AUV to collect a cohesive data set to accurately detect and track the plume edges as the plume evolves in space and time. That is, the samples taken by the AUV(s) must overlap within the plume's characteristic temporal and spatial scales to collect a synoptic data set. The importance of an ocean feature's spatial and temporal scales to feature detection and classification using AUVs is further emphasized by the work of Zhang et al. [4]. Thus, in this paper, we address the motivation for and challenges of constructing a network of AUVs to perform plume boundary tracking over two dimensions in space (horizontal) with time variations. We have chosen to track the boundary of a plume, rather than its center or maximum concentration, because the boundary gives a complete picture of the plume's spatial extent in the horizontal plane, where it is most likely to intersect a coastline or get entrained by currents and carried to another part of the ocean. We also present a simulated plume environment sampled by AUVs, from which we attempt to reconstruct the plume as a sum of Fourier orders as an initial estimate of the plume shape. The example of an oil leak, such as that from the Deepwater Horizon disaster in the Gulf of Mexico in 2010 [1], will be used to motivate a number of numerical assumptions in this paper, though we try to keep this first-pass plume simulation as general as possible to other types of plumes as well.

In addition, it is useful to know a bit about the AUVs we are using to guide numerical values for AUV simulation. For most field trials and autonomy testing, our group in the Laboratory for Autonomous Marine Sensing Systems at the Massachusetts Institute of Technology uses two Bluefin 21″ AUVs (21″ hull diameter, ~3 m in length), as shown in Figure 1. These vehicles demonstrate the best motion and stability control at speeds between 1 and 1.8 m/s, with navigational error of about 1%–5% of the distance traveled between surfacing to get a position fix via GPS. The AUVs navigate using a Leica DMC-SX Magnetic Compass and a Crossbow AHRS (attitude heading reference sensor). The navigational error quoted above assumes the AUV has constant DVL (Doppler velocity log) bottom lock, has completed a compass hard iron/soft iron calibration and has completed a compass star maneuver (for compass calibration in the water). Beyond this, the Bluefin software on the AUV also does some calibrations and math to improve the navigational accuracy to achieve the range above. To maintain reasonable stability control and navigational accuracy, the AUVs are usually commanded to travel at 1.5 m/s (though this speed varies due to autonomous adaptation to the AUVs' situations) and surface for a GPS position fix every 30 minutes, resulting in about 50–100 m of navigational error. Other instrumentation currently on board consists of a conductivity-temperature (CT) sensor, a pressure sensor, and an acoustic modem with transducer; however, these vehicles could also be equipped with sensors that measure chemical tracer concentrations or biological (Chlorophyll-a, colored dissolved organic matter, etc.) concentrations for the purposes of detecting oil, hydrothermal vent fluid, or algal concentrations. For communicating with the AUVs (Sections 3.3 and 4), we make extensive (and nearly exclusive) use of an acoustic communication structure (AUV-to-AUV and AUV-to-ship/lab) that has been actively developed and refined in recent years to give virtually real-time updates (delays on the order of minutes) of scientific and navigational data (more details on this are found in the Goby project documentation [5, 6]). Linking all of these pieces together is the autonomy system on board each AUV. This includes the Mission Oriented Operating Suite (MOOS) and the IvP Helm (IvP stands for Interval Programming), which coordinate to implement the execution of autonomy behaviors by the AUVs. These behaviors autonomously and adaptively control the heading, speed, and depth of the vehicle, depending on the behavior the AUV operators have chosen to run (more on this in Section 4 and [7, 8]).

Figure 1: One of the Bluefin 21″ AUVs operated by the MIT Laboratory for Autonomous Marine Sensing Systems.

2. Spatiotemporal Aliasing Problem

One of the most common challenges of working with AUVs to track ocean features is that of spatiotemporal aliasing, that is, when the samples taken are too far apart in space and/or time to be able to resolve the boundaries or position of a dynamic feature at a given point in space and time. This is effectively a trade-off between data coverage and data resolution. There are two extremes here (for example).

(1) A single AUV can survey a small area (~O(1 km), low spatial coverage) with very high spatial sampling resolution (>O(1 sample/m)) to resolve small-scale features in the water, such as pockets of turbulence. However, this survey would not have great enough coverage to determine the bounds of a 10 km wide algal bloom encompassing the sampling area.

(2) A single AUV can survey an area once over a long time period (≥O(10 hr), high temporal coverage) for hydrothermal vent plumes. However, it may take so long (>10 hours) to perform a spatially comprehensive survey, as witnessed by Jakuba et al. in [9] that the plume has advected away from its initial surveyed position during that period (poor temporal resolution), and the survey must be redone with less coverage to resolve the motion of the plume.

Somewhere in the middle of the above "coverage versus resolution," scenarios resides a delicate balance in which the characteristic scales of a dynamic feature (say, a plume of oil) coincide with (one-half) the rate at which the feature is sampled. This is essentially a sampling of the plume at its spatial and temporal Nyquist frequencies to maximize both coverage and resolution of the plume within the data set. Thus, it is necessary to know the characteristic spatial and temporal scales of the feature of interest for more intelligent path-planning purposes (see Figure 2), most likely involving multiple AUVs for tracking mesoscale features that are dominantly dynamic in two or more dimensions of space or any feature highly dynamic in time (such that an AUV moving ≤2 m/s could not keep up).

The necessity for designing a multi-AUV network to implement more intelligent and efficient mission planning is highly motivated by this aliasing problem, and relevant methods used by Willcox et al. and Zhang et al. to optimize AUV surveys and motivate the use of solo and multiple AUVs in efficient spatiotemporal ocean sampling and feature tracking will be important to take into account in implementing robust plume-tracking algorithms and techniques on board AUVs [3, 4].

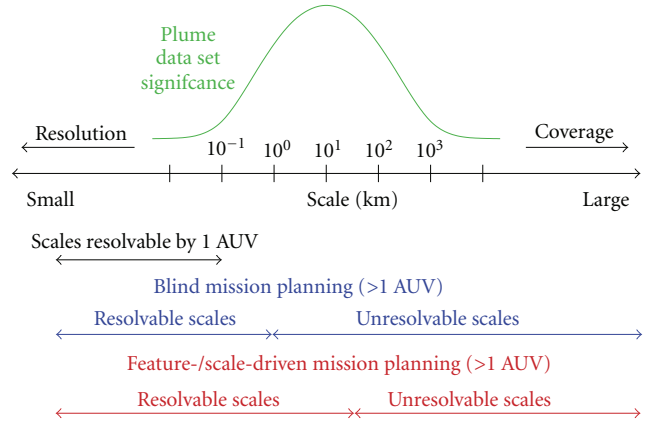

Figure 2: This figure depicts the characteristic length scale (in km) of an $O(1\,\text{km})$ plume in the horizontal plane. A similar figure can be drawn for the temporal dimension based on the characteristic time scale of a plume (with units of time). If we assume a plume has an approximate Gaussian distribution over its characteristic length scale, as shown here, we must plan AUV missions, such that the collective sampling of our AUVs overlaps with the primary length scale of the plume to optimize over coverage and resolution ("feature-/scale-driven" mission planning). This will improve the range of resolvable length scales in the resulting data set over that of "blind" mission planning, especially when the AUVs' distribution is "driven" by the characteristic spatiotemporal scales of the plume. Adapted from [12].

3. Advantages and Challenges of an AUV Network

3.1. Working as a Team. An AUV network allows for the dynamic interaction of multiple AUVs to better adapt to dynamic features in the marine environment. That is, a network of AUVs has the ability to distribute its nodes around the entire boundary of a plume and move with the plume boundary, whereas a solo AUV may be optimally placed for sampling within a plume but could not determine the horizontal spatial extent of a plume and track it simultaneously on its own. Using the estimated characteristic scales of the plume (from satellite imagery, past surveys, or physics-based calculations) in guiding the AUV autonomy behaviors (described in Section 4), the network of AUVs can be distributed in space and time to detect and track the plume boundary and avoid aliasing the data. This desire for adaptive feature tracking also underscores the necessity for using mobile (self-propelled) sensing platforms instead of, or in conjunction with, fixed and drifting sensing platforms (e.g., buoys, Argo floats), such that sampling is performed more efficiently (minimizing overlapping data), and the scientist can be certain that he/she has captured a complete data set describing the plume.

3.2. Autonomous Coordinated Control. The brains behind coordinating a sophisticated network of AUVs for plume tracking is the underlying autonomy system that must run on board each AUV. An autonomy system, such as that described in Section 4, allows an AUV to adapt to its environment in near real time, without human intervention. A few of the minimum requirements of using and interacting with a robust autonomy system are inter-AUV (acoustic) communications, support for (user-supplied) adaptive autonomy behaviors to be executed by the AUVs, and an intelligent (autonomous) means of deciding which behaviors have priority during a given mission. We propose a tiered mission planning structure for this system in which the large-scale, overall mission drives the initial formation of the AUVs (assigning each an initial position) and then allows each AUV to use individual autonomy behaviors to follow the plume edge in its local vicinity. After a period of time, the local data collected by all AUVs is then exchanged across the network to update the plume model and, subsequently, the large-scale mission of the AUVs. From here, the overall mission, to local missions, to data collection, exchange, and reprocessing loop continues for as long as required by the scientist/user.

3.3. Acoustic Communication. One of the primary challenges of using multiple AUVs simultaneously in the underwater environment is that of communication. Radio frequency (RF) waves are quickly attenuated in the water within a few meters of the surface, leaving acoustics as the primary method of real-time underwater communication. Until now, there have been few (if any) options for intelligent multi-AUV (>2 AUVs) acoustic communication schemes, though the Goby underwater communication and autonomy project (version 2.0) strives to remedy the need for coordinated message queuing and passing between multiple (and potentially an unknown total number of) AUVs [5, 6]. This will allow each AUV to discover and communicate with neighboring AUVs and share data and knowledge with the sensing platforms in its underwater network. As this part of version 2.0 of the Goby project is still in development, it is currently undergoing initial field testing and will hopefully come into use in the next year.

It is important to note, however, that plumes are often mesoscale features or larger, and AUV-to-AUV and AUV-to-ship/lab acoustic communication (at least in the public domain and on power-limited AUVs) is only possible up to a range of about 10 km. Our group at MIT has found that our equipment is usually limited to about 2 km of acoustic communication range in the coastal ocean and lake environments we have performed most experiments in recently. Our Bluefin 21″ AUVs and lab setup, which are each equipped with a WHOI Micromodem and model WH-BT-2 28 kHz transducer, transmit data in the frequency band of 23–27 kHz, centered around 25 kHz [10]. There are two realistic solutions to the acoustic communication range restriction we experience. The first and more complex solution is to implement a multihop acoustic communication scheme in which data from one AUV is passed down through a chain of AUVs to its destination. This is time consuming due to the nature of sending and listening for transmitted data packets, one at a time between communicating AUVs. Given that AUVs will often be hundreds of meters apart or more and sound speed propagation is about 1500 m/s in the ocean, data packets take an observable amount of time to transmit through the water ($O(1\,\text{sec})$). This method would also require extensive research into data routing on dynamic and time-scheduled messaging networks. The second and more immediately feasible (potentially more reliable) solution would be to restrict communication of large environmental data sets to RF or satellite methods while an AUV is on the surface and utilize a delay tolerant network rescheduling scheme. Although this method removes much of the real-time underwater data passing between AUVs (with the exception of basic position updates of nearby AUVs for avoiding collisions), it would take a large burden off of the acoustic channel and still allow each AUV to be redirected based on the most current overall picture of the plume while still performing solo autonomous and adaptive plume boundary tracking in its local vicinity in real time. Periodic surface communication would work best in the case that the AUVs can surface with great enough frequency (within the characteristic time scale of the plume) to be re-directed to a more optimal sampling position but with low enough frequency that the plume tracking mission is not significantly disrupted by the AUV taking the time to come to the surface more often.

3.4. Data Fusion. The fusion of data both from multiple sensors on a single AUV and all sensors across all networked AUVs is crucial to the success of coherently adapting a fleet of AUVs to track an ocean feature and collect a synoptic data set. When fusing data from a single vehicle, the largest concerns are keeping all data accurately time and position stamped. Across multiple AUVs, the data must also be quality checked for corruption during transmission after passing it from one vehicle to the next. It is proposed that onboard each AUV, the computer must mesh the data sets from all AUVs into a single data set, sorted over the times and positions at which each data point was taken, for each variable (i.e., temperature, salinity, etc.). Upon processing of these data on board (as on board processing is the only way to adapt to a dynamic environment in real time), for each variable, probability weighting functions over time and space must be applied to each data point based on the characteristic spatiotemporal scales of that variable. We prefer to use a basic Gaussian-shaped weighting function for this task. This will associate, say, all temperature readings taken in the last few minutes and within a radius of a kilometer horizontally (assuming the AUV can resolve its position with even better accuracy), but will ignore any temperature readings that fall outside of these ranges as independent from those inside. This essentially creates an overlap of data within a radius of one standard deviation about the sample point, as sketched in Figure 3, that can be used to prevent insufficient sampling in a data set. This data fusion method could be implemented using an SQLite (or similar) database on each AUV to compound and sort all of the environmental data from all AUVs, which may then be processed in a mathematics program such as MATLAB or Octave, or by a simple C++ parser with algorithms utilizing C++ vector math libraries. This is similar to creating an evidence grid of the AUVs' environmental data [11]. The resulting ocean environment reconstructed through data fusion with weighting can guide the mission planning for a fleet of AUVs tasked to track a plume. The AUVs can survey an area with high enough resolution to find the boundary of the plume, approximate the plume shape (see Section 5) with higher weighting near the actual sample points, and revise their coordinated survey strategy based on this new estimate of the plume boundary position.

4. Adaptive Behavior Implementation

When conducting field experiments with AUVs (usually only 1 or 2) in the water, our group at MIT runs the Mission Oriented Operating Suite (MOOS) as the underlying autonomy system on board the AUVs and on our topside mission-command computer. MOOS provides a publish-subscribe architecture that essentially deals with information sharing between autonomy processes and behaviors on board each AUV, as well as through the water between the AUVs and the topside computer [7]. To add some intelligence to the system, the IvP Helm (IvP stands for Interval Programming) is used in conjunction with MOOS to implement the use of autonomy behaviors (e.g., vertical yo-yos, trail-an-AUV, horizontal racetracks, and safety behaviors) on the AUVs, optimizing over a vehicle's speed, heading, and depth [7, 8]. The acoustic communications are handled through the Goby (stable version 1.0) autonomy software on all platforms, where it schedules the transmissions of each node (AUVs, communication buoys, topside operator, etc.) in the network [5, 6]. Goby encodes data on one node, initializes the data transmission through the acoustic channel, and then decodes the data when they are received on another node. All of these pieces to our autonomy architecture allow our AUVs to adapt their motion based on sensor readings, without a human in the loop. This allows for ocean feature detection and tracking by AUVs to occur both autonomously and adaptively, as demonstrated in the following examples.

4.1. Thermocline Tracking as a Proof of Concept. The aforementioned autonomy system has been put to the test in

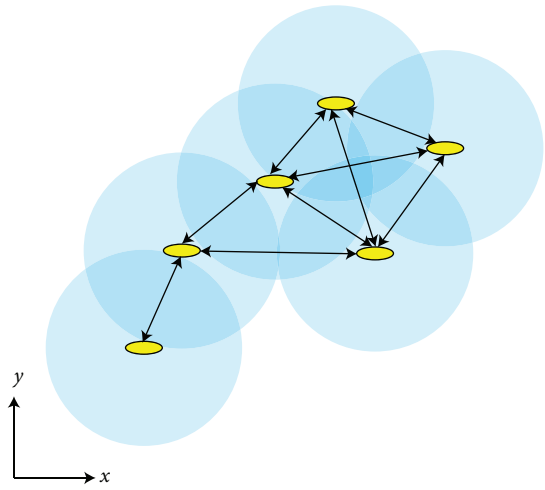

Figure 3: Blue circles around AUV sample points represent the range of significant data association possible (the radius of standard deviation of the Gaussian distribution). For any two AUV samples with overlapping range circles, an arrow is drawn to represent the fusion of data between those positions, which may be used to construct a larger-scale ocean data model when chains of fused data are combined to form a web of unaliased connections.

performing autonomous, adaptive thermocline tracking in the Tyrrhenian Sea (Italy) and Lake Champlain (Vermont, USA). As described in [13], a simple thermocline-tracking algorithm, which also accounts for the characteristic scales of the thermocline, has been developed and tested over the past few years using single AUVs of varying manufacture. Figure 4 is a conceptual sketch of the adaptive thermocline-tacking process, while more detail can be found in [13]. The idea here is that the thermocline, which is a feature only qualitatively defined in most oceanographic literature, must be quantitatively defined using actual data in real time for more efficient and adaptive oceanographic sampling. Here, it is assumed that the thermocline is relatively homogeneous in horizontal space within the AUV's operational region (for our vehicles, usually about 25 km^2 or less). That is, given an AUV's temperature measurements through the water column, on-board processing of the temperature data is accomplished spatially in 1D by binning the temperatures by depth ranges smaller than the characteristic (vertical) length scale of the thermocline in the experimental area ($O(10\,m)$ in shallow water) and using finite differences to determine the region of greatest change in temperature over change in depth. The characteristic time scale of shallow water thermoclines (in the regions this algorithm has been tested) was determined by observation during our field trials to be $O(1\,hr)$. Thus, temperature measurements were averaged over windows of 30 minutes to smooth out small local variations and spurious data points. Once the thermocline region has been determined by the AUV, the AUV will autonomously adapt its depth range to stay within the current boundaries of the thermocline and continue to collect a synoptic data set through the thermocline without expending extra energy to dive unnecessarily deeper or shallower.

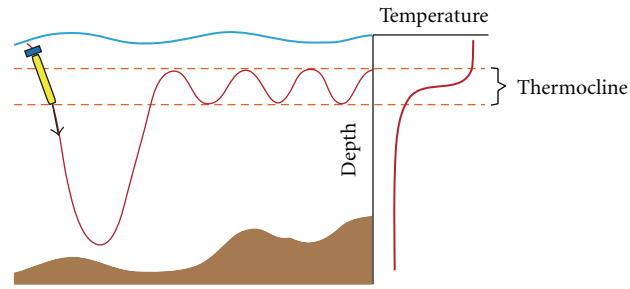

Figure 4: A conceptual sketch of an AUV performing thermocline tracking. The AUV completes a dive from the surface to as deep as allowable, collecting temperature data. The depth range of maximum temperature change per unit depth is determined as the thermocline region. The calculated upper and lower bounds of the thermocline region are then used to bound the vertical yo-yos of the AUV, essentially tracking the thermocline region. Used with permission from [13].

The successful field testing of this thermocline tracking process serves as a proof of concept for the feasibility of performing adaptive, autonomous feature tracking with an AUV, guided by the feature's spatial scale in 1D (vertically) and temporal scale to drive intelligent and efficient data collection. Thermocline tracking provides a solid first stepping stone into the field of multidimensional oceanographic feature tracking, from which we can move on to implementing applications with more complex features (dynamic in 2D or 3D space, and time) such as underwater plumes.

4.2. Plume Tracking. Plume detection and tracking using AUVs has come to the forefront of the oceanographic research community in recent years through the impacts of HABs and oil spills on coastal populations and the intrigue of studying the alien environment in the vicinity of hydrothermal vents. Smith et al. use a regional ocean model to predict the advection of a patch of water representing a HAB off the California coast, which is tagged by an actual Lagrangian drifter to passively mark and track the centroid of the imaginary HAB. AUVs (gliders) are then deployed to arrive at waypoints on the approximate boundary of the HAB when the HAB is predicted to reach that point. The calculated arrival paths of the AUVs are based on the plume boundary predictions from a regional ocean model, and the waypoints of the gliders are updated every few hours based on the previous dive's data and the model's predictions of the future boundary location of advecting the patch of water [14]. Similarly, Das et al. use satellite and high-frequency (HF) radar data sets to determine the location of high-concentration HAB patches and target these "hotspots" using AUV- (glider-) path-planning algorithms guided by the paths of the drifter tags for finer resolution sampling [15]. In a second paper, Das et al. expand this HAB tracking method further to perform Lagrangian observation studies in which the AUVs' (gliders') survey paths are precalculated to survey an advecting patch of water in its Lagrangian frame of reference to maintain sufficient spatial and temporal data resolution [16].

The difference between the aforementioned works and the implementation methods in this paper lie in the ability

of the propelled AUVs we propose to use to exhibit much better navigation control, faster speeds, limited but sufficient acoustic communication while underwater, entirely onboard data processing, and real-time feedback and reaction to sensed changes in the ocean environment without a human in the loop (no path-planning algorithms or predetermined paths/waypoints fed to the AUVs by scientists), which makes the AUVs truly autonomous and adaptive. This is, of course, at the cost of the battery duration of the AUVs, which must be recharged much more frequently. Since complex dynamic ocean models are often very large, it is not realistic to run them on board AUVs that must be fully autonomous. Satellite and HF radar images are only useful for detecting plumes with surface expressions, eliminating their usefulness in detection of neutrally buoyant plumes below the top 10 m of water. Thus, we seek to develop a method of plume tracking that can rely solely on the environmental data collected over space and time by the AUVs. The only caveat here is the assumption that a single initial large-scale survey has already been done by an AUV or other sensing platform (or a recently updated regional ocean model has been run) in the region encompassing the plume, such that an approximate plume boundary location at the plume's neutrally buoyant depth is known at the time of AUV deployment. The details of obtaining this initial plume boundary location are beyond the scope of this paper.

As mentioned in Section 3.1, it is useful to approach plume tracking by knowing something about the general dynamics and characteristic scales of the plume as well as any information about its source (for oil leaks or hydrothermal vent sites) or ocean conditions necessary for occurrence (for HABs), and what data values from various sensors might signal that a measurement was taken inside a plume. As mentioned above, since there are many approaches to first detect a plume that are beyond the scope of this paper, we will assume here that the initial 2D boundary of the plume in the horizontal plane has been detected or approximated via satellite imagery, recent oceanographic surveys, or the physics of the region of interest before any AUVs are deployed to track the plume. We will start by concerning ourselves with the horizontal extent of the plume at its neutrally buoyant depth, over a time span shorter than the plume's characteristic time scale (over which the plume boundary displays only minor variations in position). From here, we can sample the plume boundary (defined by a threshold chemical or biological concentration value during field experiments) with varying numbers of AUVs and estimate the plume shape as a sum of Fourier orders.

With an estimation of the location of a plume boundary at a given depth, multiple AUVs (preferably enough to maintain slightly overlapping one-standard deviation spatial-scale range circles along the plume boundary within the plume's characteristic time scale, similar to the range rings in Figure 3) can be deployed within the plume, and an algorithm can be used to assign each AUV a starting position near the estimated plume boundary with approximate equal spacing azimuthally between AUVs about the estimated plume center point. This initial AUV spacing can be written into an IvP Helm "equal azimuth angle" autonomy behavior that would attempt to maintain equal azimuthal spacing of the AUVs, even as they progress along the plume boundary and the boundary shifts position, adjusting the speed of each AUV to compensate if any one gets too far ahead or falls behind. A second tier of autonomy control will govern the reactions of each AUV to its local environment with a "plume boundary tracking" behavior. This behavior will have a threshold concentration value set for whatever tracer is used to signify levels of chemicals or biological productivity indicative of the plume of interest. The plume boundary tracking behavior will direct the AUV to zigzag horizontally back and forth across the position of this threshold (as it travels azimuthally around the plume center) to maintain an up-to-date position of the local plume boundary. Finally, on a time interval sufficiently small (less than the characteristic time scale of the plume) to average these data over time from each vehicle, each AUV will share its collected plume boundary position data with the other AUVs in the vicinity via acoustic (or RF or satellite) communication, and each vehicle will sort and process the collective data to determine the most current plume boundary position by estimating it as a sum of Fourier orders. Each AUV can then determine if it needs to adjust its speed and big-picture position about the plume edge using the equal azimuth angle behavior. Not only will this method of plume tracking capture the shorter/smaller-scale variations of the plume from one time interval to the next, but also create a continuously evolving track of plume evolution in space and time for a given depth.

With further development to track a plume over longer time scales, we will be able to detect the radial expansion rate of the plume boundary (if any) and its development due to advection, diffusion, and/or biological processes and thus forecast its motion to improve forward-looking mission planning. The best way to develop this plume-tracking process is through simulation, as described in Section 5. Once the simulation is complete, we will be able to initialize implementation of autonomous and adaptive plume tracking with our autonomy architecture by simulating AUVs, (acoustic) communication, and data fusion as described in Section 3 until the plume tracking algorithms and their supporting autonomy behaviors are robust enough for field testing.

5. Plume Simulation Environment

Towards the goal of developing plume-following strategies for AUVs, we must first get a sense of the characteristics of a plume and what the best method is in distributing AUVs about the plume. This requires examining the results and errors associated with reconstructing the shape of a simulated plume from simulated AUV sample points along the plume's edge. Instead of diving into incorporating a more robust or dynamic plume model developed by an outside group, we choose to simulate a very simple plume boundary in horizontal space using Fourier orders (a rough 2D plume approximation) such that we could exactly reconstruct the original plume (again by using Fourier orders) under ideal (though very unrealistic) conditions. This gives us validation that our plume reconstruction algorithms were derived correctly. Though we introduce a few sources of

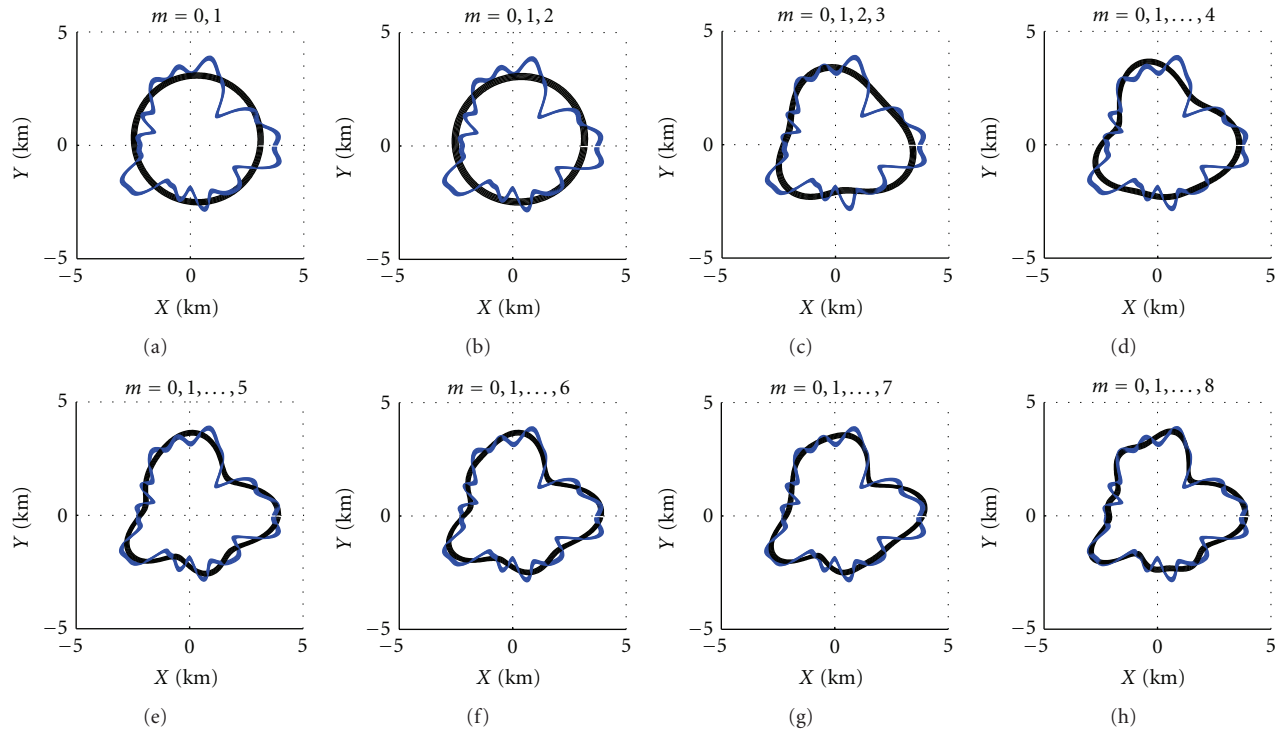

FIGURE 5: A progression of simulated plume shapes (black) of $R = 5$ km, building up to $M_{\text{hi}} = 20$ (blue).

plume reconstruction error in the plume simulation and reconstruction process described in this and subsequent sections, we expect to incorporate a more realistic, already developed plume model in the near future such that we are not setting up a situation in which our simulation is doomed to (mostly) succeed. As this is a first-pass simulation experiment, the effects of advection, dispersion, diffusion, holes in the plume shape, multiple plume sources, algal life cycle dynamics, and other complexities that may influence a plume's development over time are beyond the scope of this paper. To test our algorithms and experimental setup over a simulated characteristic plume time scale, we expand the plume in the horizontal plane over a short period of time, sample the plume boundary with varying numbers of AUVs (approximating navigation errors), and then reconstruct the plume from these time-varying sample points. This process is described below.

5.1. Modeling a Plume. A rough estimate of a plume boundary in the horizontal plane is achieved using Fourier orders of the form

$$\Phi_{M_{\text{hi}}} = \sum_{m=0}^{M_{\text{hi}}} [A_m * \cos(m\theta + \phi_m)] + R, \tag{1}$$

where M_{hi} is the highest Fourier order of the series (here, we will solve for a plume of $M_{\text{hi}} = 20$ orders by estimating it with up to 8 Fourier orders from AUV sample points), A_m is the radial amplitude perturbation of the plume boundary for the mth order, ϕ_m is the phase shift of the mth order, and R is the unperturbed radius of the plume. The angles, θ, are in the range $[0, 2\pi)$ rad about the center of the plume, and $\Phi_{M_{\text{hi}}}$ is the radial distance to the edge of the plume from the center at each angle, θ, for a maximum Fourier order, M_{hi}. Generating coefficients A and ϕ at random for each m results in the progression of plume development shown in Figure 5, leading to the overall "actual" plume in Figure 6. We have bounded A_m to $\pm R/2m$, placing the most energy in the lower orders to somewhat realistically represent the amplitude variations of the plume and minimize sharp radial inversions in the boundary shape.

Although it is possible to solve for a very large number of Fourier orders (given enough AUVs over time), this is not computationally efficient and (as seen in Section 5.4) has diminishing returns. Using a sum of many Fourier orders, however, is the most realistic approach (in this simulation) to adding complexity to the simulated plume shape. Time variation (within the characteristic time scale of the simulated plume) is also incorporated into this model, providing more total sample points per AUV (Section 5.2). Over time scales greater than the characteristic time scale of the simulated plume, it is also possible to simulate the development of the plume through turbulent and diffusive processes as well as represent the effect of dominant currents and algae life cycles on the plume shape. Though the effects of long-term time variation have yet to be incorporated into the plume simulation, we describe a means of simulating, detecting, and forecasting basic longer-time-scale radial variations in Section 6.

5.2. Sampling a Plume. First, it is important to backwards-engineer the simulated plume as follows to be sure that the

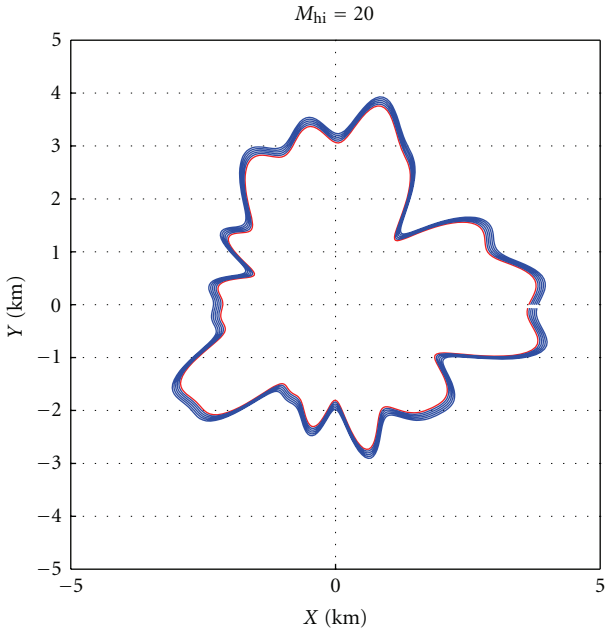

FIGURE 6: The "actual" plume of $M_{hi} = 20$ ($R = 5$ km).

AUV-sampled plume boundary reconstruction algorithms are correct. In a perfect world (with obviously unrealistic assumptions) in which a plume is exactly delineated by a finite sum of Fourier orders and AUVs are evenly spaced around the center of this sharply defined plume at a radius that is on the exact boundary (no navigational error), theory suggests that $2(M_{hi} + 1)$ AUVs are necessary to exactly solve (1) for its $2(M_{hi} + 1)$ unknowns (here, we assume that we can approximate R as the average of all AUV distances radially from the plume center, Φ_{avg}). However, since the 0th order is of constant radius, we incorporate $\cos(\phi_0)$ into A_0 and say $\phi_0 = 0$ rad, reducing the number of unknowns (and AUVs) to $2M_{hi} + 1$. Noise may be added to the angular and radial positions of the AUVs to simulate navigation error and the imperfection in trying to coordinate multiple AUVs spaced at exact angles about a circle, on the exact radius of the plume. Further error will arise from the use of a finite number of AUVs and the necessity of approximating a high order plume with an often relatively low number of Fourier orders calculated from AUV sample points. Since plumes in the ocean and in more robust plume models cannot be fully characterized in closed form as a sum of Fourier orders, error will inherently be added to the AUVs' Fourier order plume reconstruction when real data or data from a more robust model are used.

Time steps (within the characteristic time scale of the plume boundary position) may be added to increase the number of sample points available, giving $N_{samples} = N_{timesteps} * N_{AUVs}$, and to increase the maximum number of Fourier orders, $M_{AUV,max}$, that can be used to solve for the plume boundary shape. In this implementation, we applied a bounded, random, linear rate of (positive) radial expansion to the amplitude of each Fourier order in the "actual" plume, examining time steps of 2 minutes over a sufficiently small period of 10 minutes for a plume expanding radially at a rate of up to 0.5 m/s. In real-world applications, this expansion rate is based upon the vertical flow rate from the plume's source (if present, counteracted somewhat by buoyancy changes with depth) and horizontal spreading (via advection) and diffusion of the plume at the sampled depth [2]. If dealing with a HAB, the life cycle of the algae must also be considered.

5.3. Reconstructing a Plume from AUV Sample Points. Given N_{AUV} AUVs located about the plume boundary at an instant in time, at radii, Φ_{AUV}, at known angles, θ_{AUV}, a fast Fourier transform algorithm, $fft(\bullet)$, is applied to these data to determine the unknown coefficients of the plume with Fourier orders $M \leq \lfloor (N_{AUV} - 1)/2 \rfloor$. The following algorithms are then used to extract out the coefficients:

$$R \approx \Phi_{avg} = \frac{\Sigma_{\theta_{AUV}} \Phi_{AUV}}{N_{AUV}},$$

$$A_{AUV,m=0} = \frac{1}{2} * \frac{|fft(\Phi_{AUV,m=0}|_{\theta_{AUV}})|}{N_{AUV}/2} - \Phi_{avg},$$

$$A_{AUV,m=1:M} = \frac{|fft(\Phi_{AUV,m=1:M}|_{\theta_{AUV}})|}{N_{AUV}/2}, \quad (2)$$

$$\phi_{AUV,m=0:M} = \text{angle}[fft(\Phi_{AUV,m=0:M}|_{\theta_{AUV}})].$$

From coefficients $A_{AUV,m}$ and $\phi_{AUV,m}$, we reconstruct the AUV-derived estimation of the plume boundary, $\Phi_{AUV,M}$, as we constructed it in (1):

$$\Phi_{AUV,M} = \sum_{m=0}^{M} [A_{AUV,m} * \cos(m\theta_{AUV} + \phi_{AUV,m})] + \Phi_{avg}. \quad (3)$$

The reconstructed plume should match the original M_{hi}-order plume exactly (except for numerical round-off error) when all of the following criteria are met:

(i) $M_{hi} \leq M_{AUV,max} = \lfloor (N_{AUV} - 1)/2 \rfloor$, that is, the maximum Fourier order used to construct the original plume is less than or equal to the maximum Fourier order used to reconstruct it from AUV data (in reality $M_{hi} = \infty$, so this could never be achieved),

(ii) $\Phi_{avg} = R$,

(iii) there is no AUV navigation error,

(iv) there is no time variation,

(v) all AUVs are evenly spaced about the plume center and exactly on the boundary, and

(vi) there is instantaneous all-to-all communication of data.

Obviously, some error is introduced when any one of these criteria is not met. If time steps are used to increase the number of sample points, thus increasing $M_{AUV,max}$, N_{AUV} should be replaced by $N_{samples}$ in all equations in this section (Section 5.3), and the spacing of the clustered AUV samples must be interpolated to equal angular spacing about the plume edge to perform the fast Fourier transform (we have used a cubic interpolation function).

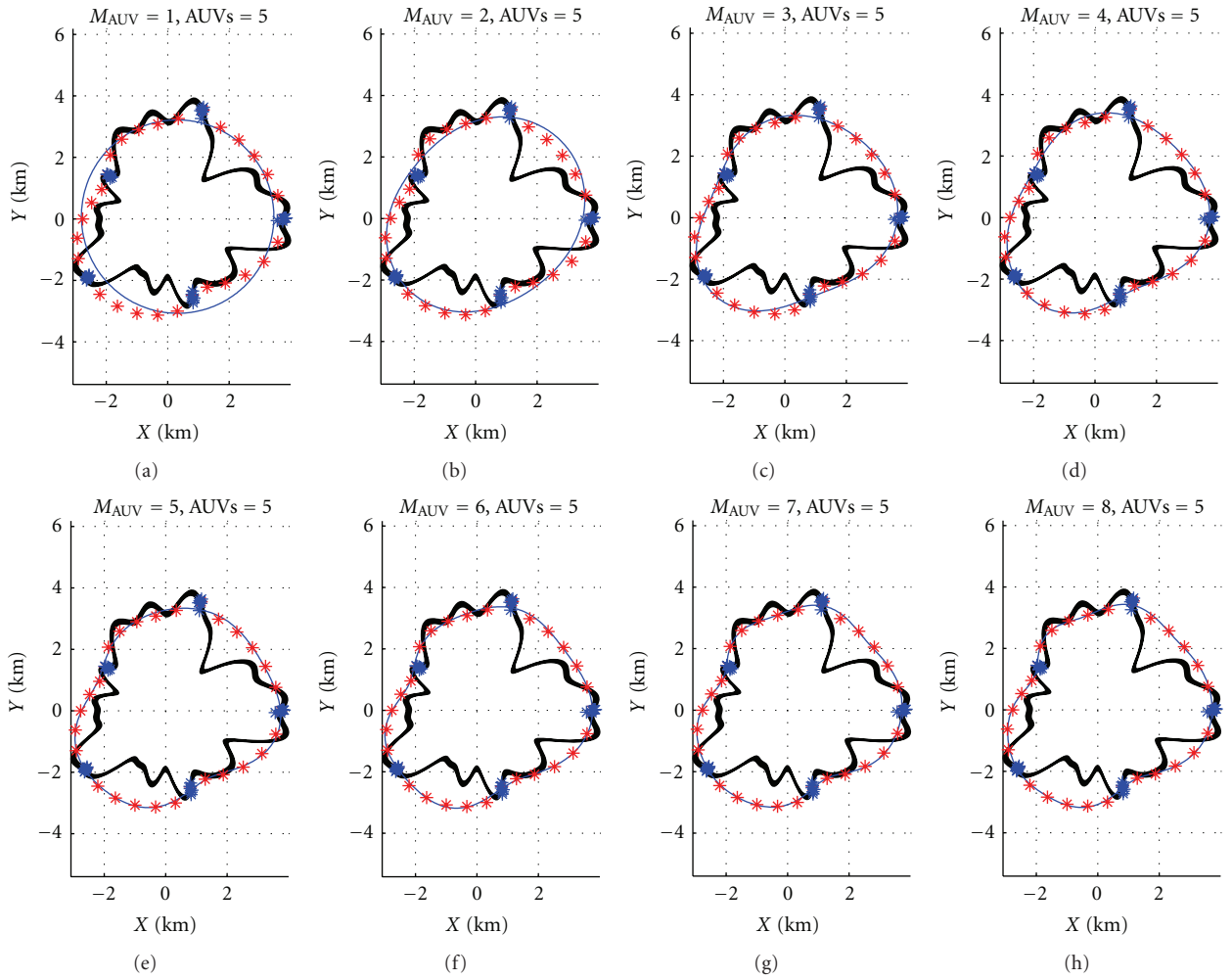

FIGURE 7: Plume estimates (blue line) of $M_{AUV} = 1, 2, \ldots, 8$ for an "actual" plume of $M_{hi} = 20$ (black lines, time varying), $R = 5$ km, navigation error = 100 m, and time steps = $0, 2, 4, \ldots, 10$ min. For the 5 AUVs, the noninterpolated (blue stars) and interpolated (cubic interpolation, red stars) AUV sample points are also shown for reference.

5.4. Results. A set of plume estimates of Fourier orders 1 through 8 are plotted in Figure 7 in contrast to the "actual" time-varying plume. These plots also show the noninterpolated (with navigation error) and interpolated AUV positions. The "actual" plume was chosen to have $M_{hi} = 20$ to keep the high-frequency variations in boundary radius to a minimum while maintaining more higher-order variation that a reasonable number of AUVs (<10) can exactly resolve. Other numerical assumptions had to be made for the sake of simulation testing and evaluation based on the Bluefin 21″ AUVs that our lab group operates and the approximate area and expansion rate of a mesoscale plume (similar to that of the Deepwater Horizon disaster in the Gulf of Mexico in 2010 [1]). Specifically, we take $R = 5$ km, AUV navigation error = 100 m, and time steps = $0, 2, 4, \ldots, 10$ min within the characteristic time scale of plume evolution.

A set of Monte Carlo simulations was used to quantify the overall mean percent error in the model based on the number of Fourier orders solved for, varying the number of AUVs while keeping the time steps consistent over all trials. This is accomplished by comparing the boundary of the estimated plume to the time-averaged boundary of the actual plume as follows:

$$\%\text{Error}_{\text{plume}} = \frac{\left|\Phi_{\text{estimated}} - \Phi_{\text{actual,time-avg}}\right|}{\Phi_{\text{actual,time-avg}}}. \quad (4)$$

These results are shown in Figure 8 for each set of Fourier orders, with $M_{AUV,max}$ determined by $N_{samples}$.

It is interesting to note that, for a fixed number of AUVs, the general trend appears to be an exponential decrease in error as a larger number of Fourier orders is solved for. However, upon closer examination of the error values, the order of lowest error is approximately $M_{AUV,min\_error} = 2N_{AUV}$. This result will help minimize the error while reasonably limiting the amount of data processing necessary to estimate the plume boundary. Alternately, for a given Fourier order M_{AUV}, as the number of AUVs increases, the percent error decreases, as is expected.

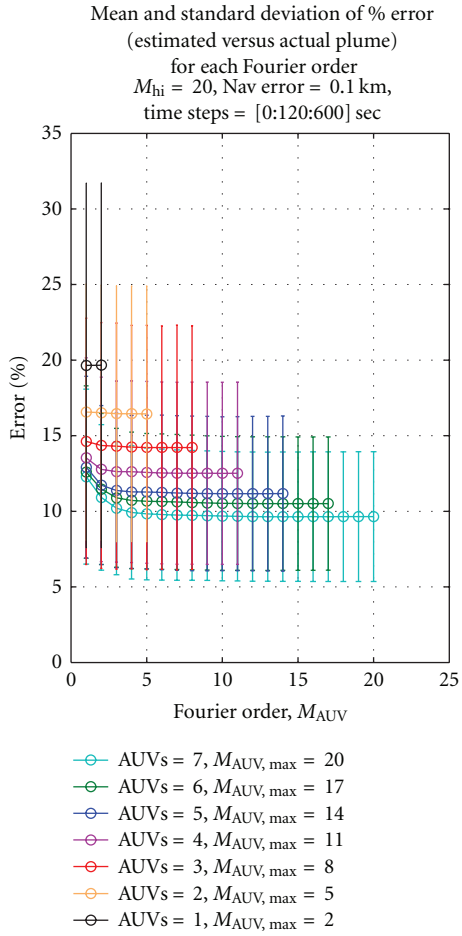

Figure 8: Percent error in plume radius between the estimated and actual (time-averaged) plumes, averaged over 500 trials. Mean values are shown for each maximum Fourier order, with error bars showing ±1 standard deviation.

6. Forecasting Long-Term Variations

Having simulated and analyzed a plume over a short time span, we will now explore expanding the plume simulation to longer time spans to enable plume shape forecasting. There are two formulations here for the basic time expansion approximation. We may either assume that the plume expands linearly in time in the radial direction, with a constant coefficient of expansion, $d\Phi/dt$ (5), or that both the amplitude and phase coefficients change linearly in time, with constant coefficients dA/dt and $d\phi/dt$ (6). These are the most simplistic cases, which may be built upon in the future into nonlinear coefficients to account for further complexities from real ocean dynamics:

$$\Phi_{M_{hi}}(\theta, t) = \sum_{m=0}^{M_{hi}} [A_m * \cos(m\theta + \phi_m)] + \frac{d\Phi}{dt} * (t - t_0) + R, \quad (5)$$

$$\Phi_{M_{hi}}(\theta, t) = \sum_{m=0}^{M_{hi}} \left[\left(A_m + \frac{dA}{dt} * (t - t_0) \right) * \cos\left(m\theta + \left(\phi_m + \frac{d\phi}{dt} * (t - t_0) \right) \right) \right] + R. \quad (6)$$

Assuming one of the above plume formulations and sampling it with AUVs over a number of large time steps, we can determine the differences in overall plume shape from one point in time to the next and back out the constant coefficients from there. If the formulation in (5) is assumed, we may simply find the mean difference (over all θs) in radius between the estimated plumes at times t_0 and t_1, as shown in (7):

$$\frac{d\Phi}{dt} \approx \text{mean}\left[\frac{\Phi_{AUV,M}(\theta, t_1) - \Phi_{AUV,M}(\theta, t_0)}{t_1 - t_0} \right]. \quad (7)$$

Solving (6) for formulation coefficients is more complex. Given estimated plumes from AUVs at times t_0 and t_1 sufficiently far apart in time, we must maximize the correlation between $\Phi_{AUV,M}(\theta, t_1)$ and $\Phi_{AUV,M}(\theta, t_0)$ over radius and azimuth angle. The tool for this will be a matched filter applied to $\Phi_{AUV,M}(\theta, t_1)$ and $\Phi_{AUV,M}(\theta, t_0)$, allowing us to back out the constant coefficients once we determine the phase and amplitude changes between t_0 and t_1. Repeating either of the above processes over multiple time steps will further improve the accuracy of the coefficients.

Once we solve for the constant coefficients using either of the above methods, a forecast can be made for the plume shape by simply applying the linear changes to the estimated plume shape at the last known time slice and projecting it forward to the next time step(s). As with any forecasting, however, the accuracy of the forecast decreases with time steps further into the future. A weighting function (potentially the right side of a Gaussian) should be included with the forecast to account for this.

7. Looking Ahead

It is important to take what we have learned from this exercise and apply it to a more robust plume simulation, such as a theory- and data-derived dynamic plume model, as well as to prepare for taking this application into the field. Following the first iteration of this plume simulation, the next step is to use the plume estimated by the AUVs over progressive time steps to estimate the linear time perturbation coefficients of each Fourier order and use these coefficients for future prediction.

Jumping ahead to prepare for realistic implementation of plume tracking in the field, we plan to use our IvP Helm and Goby autonomy to move the AUVs along the actual plume boundary (in "follow-the-leader" fashion) as described in Section 4.2, autonomously adapting their tracks to their real-time measurements by zigzagging across the boundary, and keeping their angular spacing relatively constant. As AUVs travel along the boundary azimuthally, all at the same

speed, the radial excursions in the boundary may cause the azimuthal spacing of adjacent AUVs to degrade. To counter this effect, we will employ autonomy behaviors to change speed and maintain azimuthal distribution when a significant degradation in spacing is detected. This will first be implemented in simulation to work out any bugs before taking it into the field with the AUVs.

Other features to add to the plume simulation will account for the effects of advection by currents and turbulent diffusion. A good estimation for diffusion, used widely in the underwater community, is Fick's Law [17], and examples of current effects can be found in [1, 9]. These effects may be best incorporated into the simulation as time-varying coefficients similar to those in Section 6, only nonlinear in time and space. Another option would be to take advantage of a commercial computational fluids simulator to simulate these effects. It will also be important to account for the direction of motion of a plume, as this may or may not cause the leading edge of the plume to be more distinct than the trailing edge. Again, however, we do not want to reinvent the wheel and may prefer to research and take advantage of already existing plume models and data that account for some of these effects with greater detail and accuracy than achievable by the above method. In the case of the evolution of HABs, we must also account for life cycle evolution of the algae, and testing with historical data of algal bloom evolution would be useful here [15].

Finally, it is important to gain a knowledge of how each source of error (i.e., navigation error, higher modes and sharper inversions in plume shape, overall plume radius, cubic interpolation of AUV spacing about the plume, etc.) affects the overall error in the estimated plume boundary. Such an error review will require a wide range of tests, changing only one variable at a time. The cubic interpolation of AUV position alone will be evaluated against other interpolation techniques, such as the Lomb-Scargle method [18], to minimize errors.

8. Conclusion

This paper provides a conceptual outline of the requirements for implementing adaptive, autonomous plume tracking using a network of AUVs, including a first-pass simulation of detecting and reconstructing plume shapes solely from AUV sample points, with the example of a plume of oil originating from the sea floor. Using a sum of M_{hi} Fourier orders to represent a plume shape at its neutrally buoyant depth, we added noise in the AUV positions to represent navigation error. We also incorporated linear radial expansion of the plume over time to simulate plume spreading due to the continuous influx of oil. Reconstruction of the plume from the time-varying AUV samples was seen to result in errors in the estimated versus original plume shapes ranging from 9 to 20% (for 1 through 7 AUVs, $M_{\text{hi}} = 20$, $R = 5$ km, navigation error $= 100$ m, and time steps $= 0, 2, 4, \ldots, 10$ min), largely decreasing with an increase in the number of Fourier orders being solved for, keeping the number of AUVs, navigation errors, and time steps constant. The errors also decrease as the number of AUVs is increased. With this knowledge and technology, we will be able to improve the plume simulation further based on the physics of plume spreading via currents and diffusion and employ adaptive autonomy behaviors with the AUVs to progress them along the plume boundary. In the end, the plume tracking process presented here will provide a synoptic data set describing the plume based on the spatiotemporal scales of the feature, using a network of AUVs to prevent data aliasing.

Acknowledgments

This research was made with Government support under and awarded by DoD, Air Force Office of Scientific Research, National Defense Science and Engineering Graduate (NDSEG) Fellowship, 32 CFR 168a. The authors would also like to acknowledge the NATO Undersea Research Centre (NURC) in La Spezia, Italy for all their help in organizing and conducting field trials (GLINT '09, GLINT '10) to test AUV feature tracking behaviors as well as for use of their marine assets that allowed us to build up to this research. They would like to acknowledge the US Office of Naval Research for funding portions of the necessary travel, underlying research, and sea trials. As well as the Naval Undersea Warfare Center Division, Newport (Code 25)—Technical Support and Logistics, and the Office of Naval Research TechSolutions Program Office (Lightweight NSW UUV program)—Technical Support for funding Champlain '09 and allowing us to use the Iver AUV for thermocline tracking experiments. Finally, the authors would like to thank Toby Schneider and Donald Eickstedt for numerous discussions and feedback about this and related research as well as Pierre Lermusiaux's MSEAS group at MIT for supplying ocean models, and the rest of the LAMSS group at MIT for their support of these efforts.

References

[1] R. Camilli, C. M. Reddy, D. R. Yoerger et al., "Tracking hydrocarbon plume transport and biodegradation at deepwater horizon," *Science*, vol. 330, no. 6001, pp. 201–204, 2010.

[2] J. S. Turner, *Buoyancy Effects in Fluids*, Cambridge Monographs on Mechanics and Applied Mathematics, Cambridge University Press, Cambridge, UK, 1973.

[3] J. S. Willcox, J. G. Bellingham, Y. Zhang, and A. B. Baggeroer, "Performance metrics for oceanographic surveys with autonomous underwater vehicles," *IEEE Journal of Oceanic Engineering*, vol. 26, no. 4, pp. 711–725, 2001.

[4] Y. Zhang, A. B. Baggeroer, and J. G. Bellingham, "Spectral-feature classification of oceanographic processes using an autonomous underwater vehicle," *IEEE Journal of Oceanic Engineering*, vol. 26, no. 4, pp. 726–741, 2001.

[5] T. Schneider and H. Schmidt, "The dynamic compact control language: a compact marshalling scheme for acoustic communications," in *Proceedings of the IEEE Oceans Conference*, Sydney, Australia, May 2010.

[6] Goby Developers, "Goby underwater autonomy project documentation," http://gobysoft.com/doc/1.0.

[7] M. R. Benjamin, H. Schmidt, P. M. Newman, and J. J. Leonard, "Nested autonomy for unmanned marine vehicles

with MOOS-IvP," *Journal of Field Robotics*, vol. 27, no. 6, pp. 834–875, 2010.

[8] M. R. Benjamin, J. J. Leonard, H. Schmidt, and P. M. Newman, "An overview of MOOS-IvP and a brief users guide to the IvP Helm autonomy software," Tech. Rep. MIT-CSAIL-TR-2009-028, 2009, http://hdl.handle.net/1721.1/45569.

[9] M. Jakuba, D. Yoerger, A. Bradley, C. German, C. Langmuir, and T. Shank, "Multiscale, multimodal AUV surveys for hydrothermal vent localization," in *Proceedings of the Fourteenth International Symposium on Unmanned Untethered Submersible Technology (UUST '05)*, Durham, NH, USA, 2005.

[10] Woods Hole Oceanographic Institution, "WHOI acoustic communications: micro-modem overview," 2011, http://acomms.whoi.edu/umodem/.

[11] M. Martin and H. Moravec, "Robot evidence grids," Tech. Rep. CMURI-TR-96-06, The Robotics Institute, Carnegie Mellon University, Pittsburgh, Pa, USA, 1996.

[12] D. Wang, P. F. J. Lermusiaux, P. J. Haley, D. Eickstedt, W. G. Leslie, and H. Schmidt, "Acoustically focused adaptive sampling and on-board routing for marine rapid environmental assessment," *Journal of Marine Systems*, vol. 78, supplement 1, pp. S393–S407, 2009.

[13] S. Petillo, A. Balasuriya, and H. Schmidt, "Autonomous adaptive environmental assessment and feature tracking via autonomous underwater vehicles," in *Proceedings of the IEEE Oceans Conference*, Sydney, Australia, May 2010.

[14] R. N. Smith, Y. Chao, P. P. Li, D. A. Caron, B. H. Jones, and G. S. Sukhatme, "Planning and implementing trajectories for autonomous underwater vehicles to track evolving ocean processes based on predictions from a regional ocean model," *International Journal of Robotics Research*, vol. 29, no. 12, pp. 1475–1497, 2010.

[15] J. Das, K. Rajan, S. Frolov et al., "Towards marine bloom trajectory prediction for AUV mission planning," in *Proceedings of the IEEE International Conference on Robotics and Automation (ICRA '10)*, pp. 4784–4790, May 2010.

[16] J. Das, F. Py, T. Maughan et al., "Simultaneous tracking and sampling of dynamic oceanographic features with autonomous underwater vehicles and Lagrangian drifters," in *Proceedings of the 12th International Symposium on Experimental Robotics*, New Delhi, India, December 2010.

[17] "Oceanic diffusion and mixing," http://flux.ocean.washington.edu/WQ2009/oc515.mixing.pdf.

[18] W. H. Press and G. B. Rybicki, "Fast algorithm for spectral analysis of unevenly sampled data," *Astrophysical Journal*, vol. 338, pp. 277–280, 1989.